Proceedings of the Tenth Pacific Conference on Earthquake Engineering
Building an Earthquake-Resilient Pacific
6-8 November 2015, Sydney, Australia

Experimental research on reduced beam section to concrete-filled steel tubular column joints with RC slab

R. Li, B. Samali & Z. Tao

Institute for Infrastructure Engineering, University of Western Sydney, Penrith, Australia

ABSTRACT: Steel beams are often connected to reinforced concrete (RC) floor slabs by shear connectors in real construction. Extensive studies have been conducted on joints to steel beams with Reduced Beam Section (RBS) but limited research has focused on the joints with RBS composite beams. This paper presents an experimental investigation on the cyclic behaviour of the concrete-filled steel tubular (CFST) column to RBS composite beam joints with through diaphragm. The evaluation of the influence of the RC floor slab and RBS is conducted by testing three half-scale joint specimens, including a joint with steel beams, a joint with composite beams and a joint with RBS composite beams. Combined constant axial load and cyclic lateral load were applied to specimens. The strength, ductility, stiffness degradation and energy dissipation capacity are analysed. It is found that the CFST column joint with RBS composite beams exhibits favourable seismic performance. Although the strength slightly decreases under hogging moment, both the ductility and energy dissipation capacity of joints are improved. This type of composite joint has a good prospect in seismic zones.

KEYWORDS: Concrete-filled steel tubular column; Reduced beam section; Diaphragm-through joint; Composite beam.

1 INTRODUCTION

Concrete-filled steel tubular (CFST) columns have many structural and constructional benefits. The steel tube of a CFST column normally provides the confinement to the concrete, while the concrete restrains the local buckling of the steel tube. In addition, the steel tube provides formwork for the concrete pouring during construction, which reduces the construction time. Therefore, the combined utilisation of CFST columns and steel beams has increased in composite building construction in recent years. In general, steel beams and reinforced concrete floor slabs can work together as a whole through shear connectors in real construction. Nevertheless, still limited studies have been conducted on the CFST column joints with composite beams compared with the CFST column joints with steel beams.

Cheng et al. (2007) tested four joints composed of square CFST column and steel-concrete composite beams. Two exterior joints and two interior joints with internal diaphragm were prepared. They evaluated the contribution ratio of the reinforced concrete slab in composite joints and analysed seismic properties of two joints with tapered beam flanges and lengthened shear tabs. Four interior and two exterior joints were constructed by Han and Li (2010), in which external diaphragm was welded to the circular CFST column, and then welded to the H-steel beams. RC slab was placed upon the beam flange by round headed stud connectors. All specimens were quasi-statically tested to study the seismic properties of the composite joint. Besides CFST columns, concrete encased concrete filled steel tubular columns have also been applied in real construction. Liao et al. (2014) studied seven specimens, including four joints of concrete encased CFST columns to RC beam and three joints with steel beam. It is found that the strength of joints with RC beam is dominated by beam failure. Slab enhances the beam stiffness and the ultimate strength of joint, and the failure mode might be changed when it involved floor slab.

The above literature review indicates that little attention has been paid to the composite joints with RBS composite beams. However, the RBS beam is becoming popular for earthquake resistant buildings, so it is important to investigate the seismic behaviour of joints composed of CFST columns and RBS composite beams. Thus, three joint specimens were tested, including a joint with steel

beams, a joint with composite beams and a joint with RBS composite beams. The stiffness, strength and energy dissipation of these joints are analysed and compared based on the test results.

2 EXPERIMENTAL PROGRAM

2.1 Test specimens

This test focuses on the seismic behaviour of the CFST column to RBS composite beam joints with through diaphragm. Three cruciform specimens with RC slabs are designed. **Figure 1** shows configuration of the specimens. The profiles of circular steel tubes are 250 mm in diameter with 6 mm wall thickness; the beams have a depth of 248 mm and a length of 1,600 mm from the centre of the column to the assumed inflection point at the end of each beam; the width and depth of RC slabs are 800 and 60 mm, respectively. Through diaphragms with a thickness of 10 mm were used to connect column and beam. Outer diameter, inner diameter and vent hole diameter of the through diaphragm are 300 mm, 120 mm and 20 mm, respectively. M19 headed shear studs with a length of 50 mm and a diameter of 19.3 mm are evenly welded along the steel beam to connect the steel beam to the floor slab. Details of the joint specimen dimensions and parameters are shown in Table 1, in which n is the axial load level, k_{m} is the ratio of the column flexural capacity to the beam flexural capacity considering the existence of the RC slab, and $k_{\mathrm{m}}^{'}$ is the ratio of the column flexural capacity to the beam flexural capacity without the presence of the RC slab.

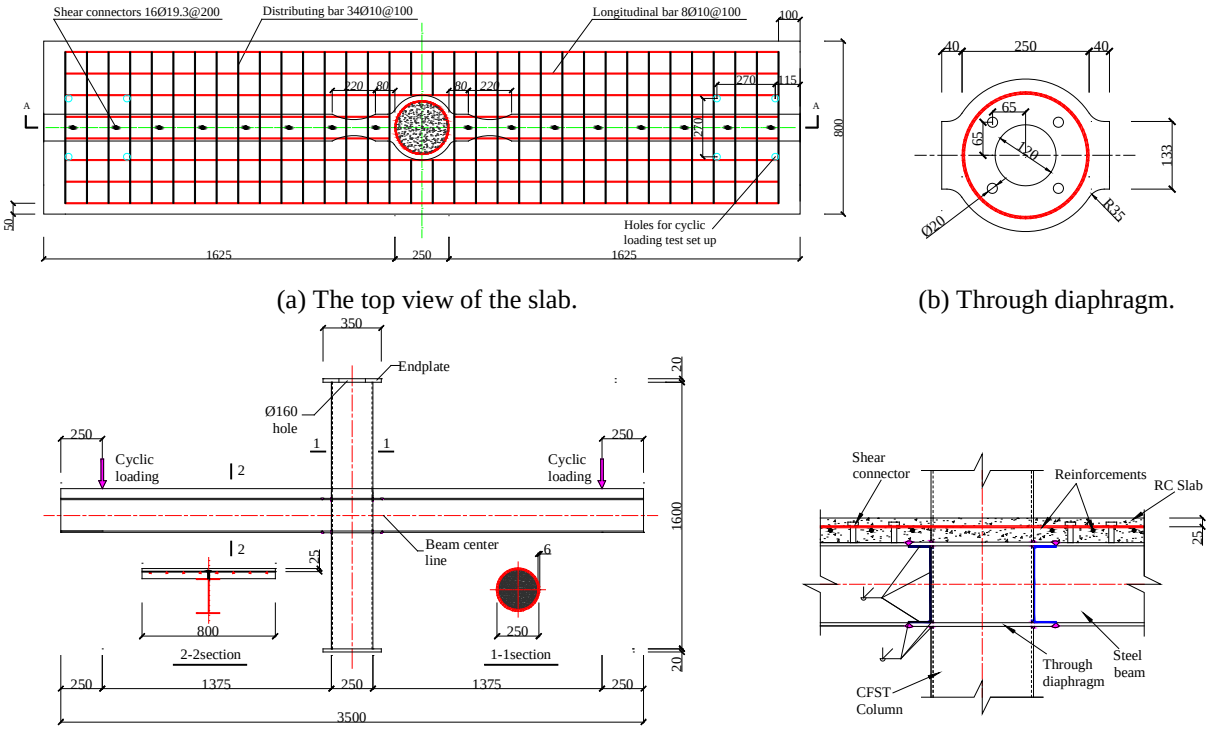

(a) The top view of the slab.

(b) Through diaphragm.

(c) Detail of through diaphragm.

(d) A-A section.

Figure 1. Configuration of the specimens.

Table 1. Details of test specimens.

Speci-mens No.	Column $D \times t_s$	Beam $h_b \times b_f \times t_w \times t_f$	Cut depth of the RBS (mm)	n	k_E	$k_{E,RBS}$	k_E'	k_m	$k_{m,RBS}$	k_m'	Slab	Predicted failure mode
CN-1	○-250×6	248×124 ×5.0×8.0	0	0.4	–	–	1.26	–	–	1.81	No	Beam
CS-1	○-250×6	248×124 ×5.0×8.0	0	0.4	1.06	–	–	0.97	–	–	Yes	Column
CS-5	○-250×6	248×124 ×5.0×8.0	31 (0.25b_f)	0.4	1.06	1.24	–	0.97	1.19	–	Yes	Beam

Specimen CN-1 was a CFST column-steel beam joint, the other two specimens CS-1 and CS-5 were joints with composite beam. Beam cross-section of specimen CS-1 was kept intact without section reduction, while beam flanges of specimen CS-5 had a cut depth of 31 mm, as shown in **Figure 1**(a). A layer of reinforcement (ϕ10 mm) was placed in the RC slab, which were evenly distributed along the slab at a space of 100 mm. The CFST columns and steel beams were the same for all three joints. The Complete Joint Penetration (CJP) groove welds were used to connect the column and beam.

Material properties

Three welded steel tubes were used for fabricating the CFST columns, as shown in **Figure 2**. Two through diaphragms were welded to each steel tube by double-fillet weld. Then the beam flanges were welded to the through diaphragms and the beam web was welded directly to the steel tube. The thicknesses of all weld seams were around 6 mm. Each end of the steel tubes was welded to a 350×350 mm steel plate; the steel plate on the top end had a ϕ 160 mm hole used for pouring concrete.

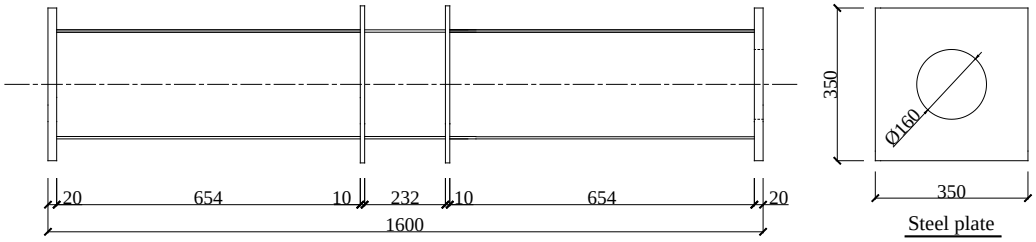

Figure 2. Detail of steel tube

Coupon tensile tests were carried out to determine the material properties of steel. The test results are listed in the **Table 1**, where d denotes the diameter, t denotes the thickness, f_y denotes the yield strength, f_u denotes the ultimate strength, E_s denotes the modulus of elasticity, and δ denotes the elongation ratio. Grade C32 normal concrete was used for the infill concrete and RC slab. Concrete cylinder tests were conducted. The measured cylinder concrete compressive strength (f_{cu}) was 36.5 MPa and the Young's modulus was 37,738 MPa at the time of testing.

Table 2. The material properties of steel.

Element	***d* or *t* (mm)**	f_y **(N/mm^2)**	f_u **(N/mm^2)**	E_s **(MPa)**	δ
Steel tube	5.96	386.6	480.4	199433	27.9
250UB flange	14.2	299.9	455.6	201516	37.6
250UB web	8.6	344.6	468.9	204120	34.3
Through dia-phragm	10.1	289.7	440.7	201745	38.3
Shear stud	ϕ12	402.3	487.5	200713	34.1
Reinforcement	ϕ10	609.7	639.6	203238	24.5

2.2 Loading protocol

Tests were carried out at the University of Western Sydney. Illustration of the test setup is shown in **Figure 3**. A constant axially compressive load of 1,116 kN (0.4N_u) was applied to the column by a hydraulic jack. The column ends were restrained from horizontal movement but allowed to rotate in the loading plane. Cyclic loads (P) in the vertical direction were applied at the tips of the two beam segments by two MTS hydraulic jacks, respectively. The cyclic displacement amplitude followed the loading protocol in SAC (1997). The deformation parameter to be used to control the loading history is the inter-story drift angle (θ), which is defined as the beam deflection divided by the beam span. The loading history is divided into several steps. Firstly, the loading starts with six cycles at each load step of 0.00375 rad, 0.005 rad and 0.075 rad rotation, respectively. The next four cycles in 4th load step are at 0.01 rad rotation, followed by two cycles in 5th load step of 0.015 rad rotation. The load sequence completes two cycles at each rotation value, followed by increasing the rotation value (0.02 rad, 0.03 rad, 0.04 rad…until failure of the joint). The cyclic loading speed is controlled at a rate of 0.5 mm/s.

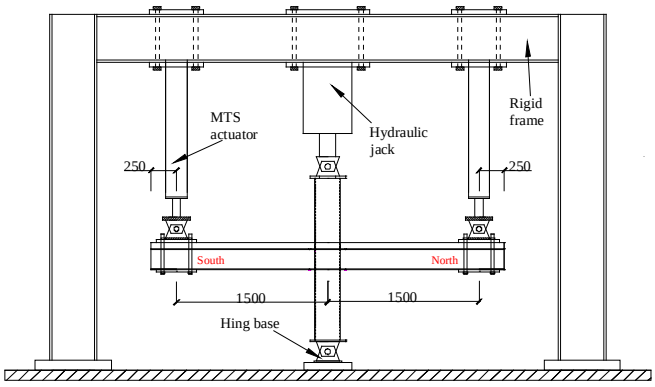

Figure 3. Experimental setup.

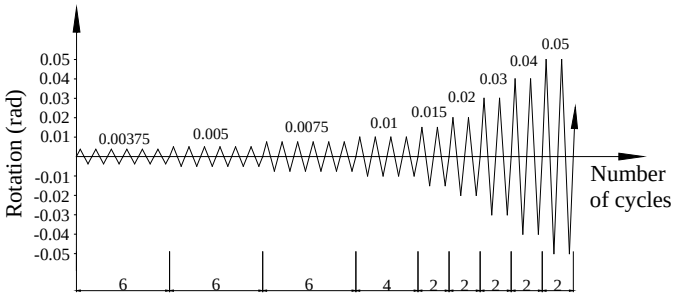

Figure 4. Typical loading protocol.

3 DISCUSSION AND ANALYSIS OF TEST RESULTS

3.1 Experimental results

3.1.1 *Joint without RC slab*

Specimen CN-1 failed by fracture of the steel beam at the end of the test. Initial yielding occurred during the first cycle of 2% rad story drift, which was observed at the south beam. Later, initiation of the flange buckling appeared close to the yielded top flange of the north beam at a drift of 4% and the whitewash of the beam web peeled off. When the displacement of the beam tip reached 75 mm (5% rad), the ultimate bending moment of the joint was observed, which was 1.18 times its yielding bending moment, as shown in **Figure 7**. At this point, load started dropping and the buckling of beams became more obvious with the increasing of the displacement of the beam tip. Finally, the test was terminated on the cycles of 8% rad story drift due to the bending moment of the joint had decreased to 85% of its ultimate bending moment. **Figure 5** shows the final appearance of specimen CN-1. Fracture was visible at the top weld seam edge, as shown in **Figure 6**.

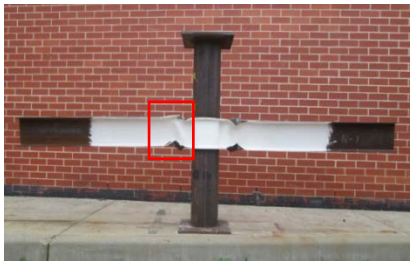

Figure 5. Final appearance of specimen CN-1.

Figure 6. Buckling of the beam and fracture of the weld seam.

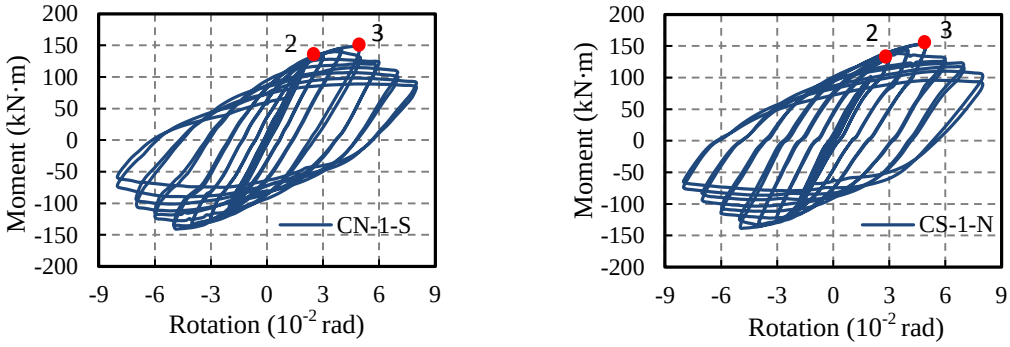

(a) CN-1-South

(b) CN-1-North

(2. Yielding point; 3. Maximum strength.)

Figure 7. *M-φ* hysteretic curves of specimen CN-1.

3.1.2 *Joints with RC slab*

Column failure and beam failure were observed for specimens CS-1 and CS-5, respectively. The first flexural crack developed on the slab surface of these two specimens close to column at a rotational angle of 0.0075 rad, and then propagated outward. The length and width of cracks expanded in the direction of slab edges with the increasing of the beam tips load. In successive loading cycles, a visual buckling occurred in the column of specimen CS-1 (on the side of the beam under hogging moment) about 30 mm below the bottom through diaphragm when the rotational angle reached 0.015 rad. As the column-to-beam bending moment ratio for specimen CS-1 was less than 1, local buckling occurred in the column before the bottom steel beam flange yielded. At a rotational angle of 0.03 rad, the local buckling became more obvious, and significant deformation of the column was observed at a later stage, as shown in **Figure 8**, accompanying with clear sounds of the infilled concrete being crushed. The test terminated due to the strength of the joint decreasing to 85% ultimate strength on the second cycle at the stage of 0.03 rad.

At a story drift of 0.03 rad, only a slight inelastic deformation occurred on the specimen CS-5, which located at the lower portion of the web of the north RBS region. Later, initiation of web local buckling was observed in the next loading step (0.04 rad story drift), indicated by the flaked whitewash paint. The strength degradation was observed at the 0.07 rad story drift resulted from a serious local buckling in the RBS region. Ultimately, the slab concrete near the column surface crushed and spalled, and then the joint failed because of the torn flange in the south RBS region, as shown in **Figure 9**.

Figure 8. Failure modes of specimen CS-1.

Figure 9. Steel fracture observed in specimen CS-5.

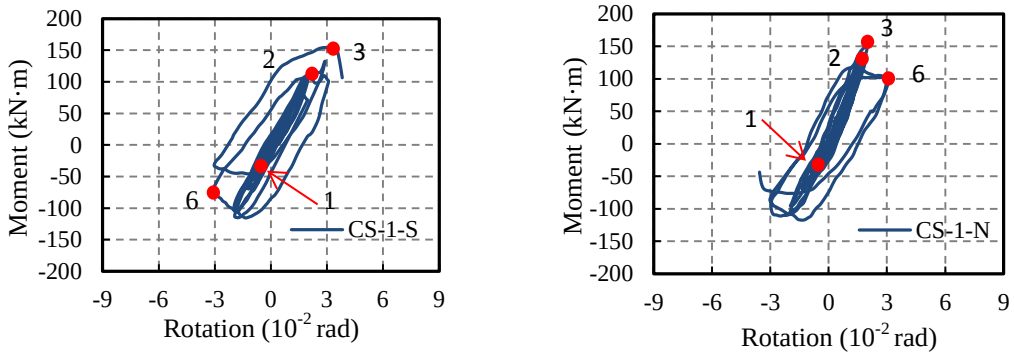

(a) CS-1-South (b) CS-1-North

(1. Crack initiation; 2. Yielding point; 3. Maximum strength; 6. Local buckling of the steel tube.)

Figure 10. *M-φ* hysteretic curves of specimen CS-1.

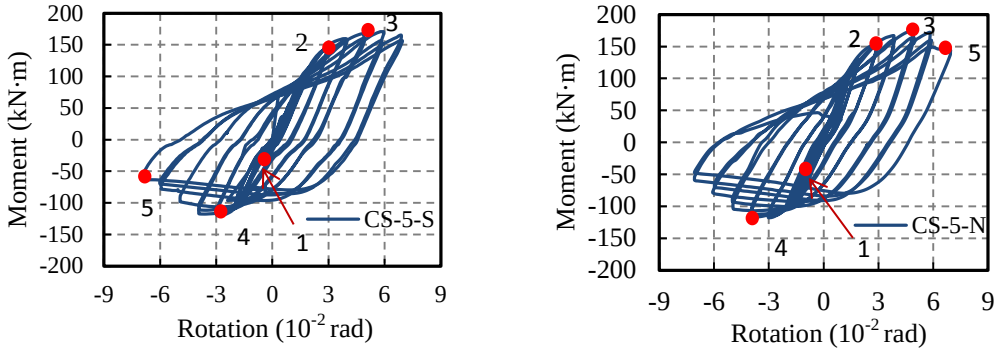

(a) CS-5-South (b) CS-5-North

(1. Crack initiation; 2. Yielding point; 3. Maximum strength; 4. Local buckling of the web; 5. Beam flange fracture.)

Figure 11. *M-φ* hysteretic curves of specimen CS-5.

3.2 **Analysis of experimental results**

Envelope curves of the hysteretic curves are shown in **Figure 12**, which are obtained by connecting the peak load points of each cycle. From the envelope curves and hysteretic curves, they have revealed that: 1). The shapes of hysteretic curves are similar, demonstrating no obvious pinch effect. 2). Owing to the presence of the RC slab, the initial stiffness and the maximum strength under sagging moment are higher than those under hogging moment, as observed in specimens CS-1 and CS-5. 3). The RBS improves the ductility of composite joints, which can be seen from **Figure 12** (b) by comparing the envelope curve of specimen CS-1 with that of specimen CS-5. Further analysis is given in the following subsections.

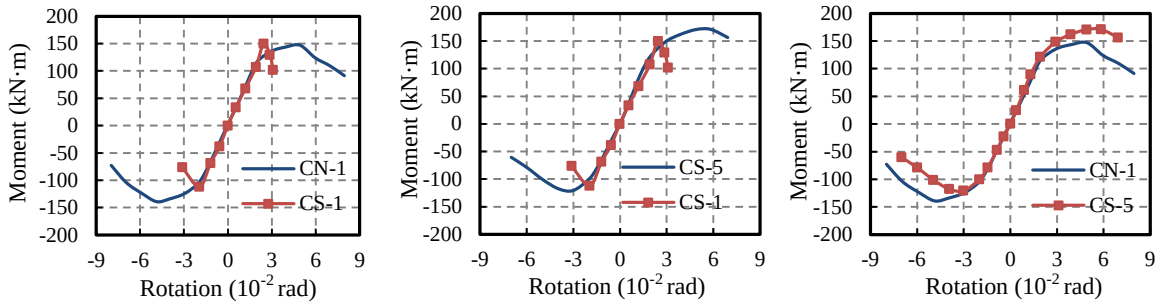

4 (a) (b) (c)

Figure 12. *M-φ* envelope curves.

Yield strength and ultimate strength are significant in structural design, but some composite materials have not an obvious yield point and ultimate point in the *M-θ* curve. Therefore, a method is selected for determination of the yield points and failure points (Han & Li, 2010), as shown in **Figure 13**. **Table 3** shows the summary of the measured results. The displacement ductility coefficient (μ) is defined as θ_u/θ_y to reflect the ductility of composite connection specimens, where θ_u and θ_y are the rotations correspond to the failure and yield points on *M-θ* skeleton curve.

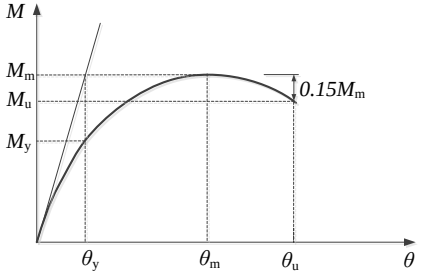

Figure 13. The method to estimate the yield, ultimate and failure points.

Table 3. Summary of measured results.

Specimen	M_y		M_m		M_u		θ_y		θ_m		θ_u		μ		$\bar{\mu}$
	(+)	(-)	(+)	(-)	(+)	(-)	(+)	(-)	(+)	(-)	(+)	(-)	(+)	(-)	
CN-1	123.4	-117.7	147.1	-139.1	124.9	-118.2	2.3	-2.5	4.9	-4.9	5.8	-6.4	2.52	2.56	**2.54**
CS-1	143.2	-91.3	149.9	-112.1	127.5	-95.3	2.4	-1.7	2.5	-2	2.9	-2.5	1.21	1.47	**1.34**
CS-5	136.3	-98.9	171.1	120.5	156.3	-102.5	2.4	-1.9	5.8	-3	6.9	-4.9	2.88	2.58	**2.73**

3.2.1 *Effect of RC slab*

It is expected that the existence of the RC slab can enhance the strength and stiffness of the composite joint, and the ratio of the column flexural capacity to the beam flexural capacity will decrease. Due to the change in the above ratio, the presence of the slab indeed changed the joint failure mode from beam failure mode (CN-1) to column failure mode (CS-1). But compared with the reference specimen CN-1 without slab, specimen CS-1 had only marginal strength increase in sagging moment and even a decrease in hogging moment by 19.4%. This is mainly due to the premature failure of the CFST column in specimen CS-1. After the test, partial steel tube of specimen CS-1 was removed and significant defects were found in the concrete just below the bottom through diaphragm, as shown in **Figure 8**. This highlights the fact that special care should be taken to place concrete in steel tubes with existence of through diaphragms. However, the yield moment of specimen CS-1 (143.2 kN·m) was still higher than that of specimen CN-1 (123.4 kN·m) under sagging moment, which indicates the positive influence of the RC slab on the joint strength. **Figure 12** (c) compares the envelope curves of specimens CS-5 and CN-1. Although RBS beam was used in specimen CS-5, compared with the reference specimen, the ultimate sagging moment of CS-5 still increased by 16.3% due to the presence of the slab. But the hogging moment of specimen CS-5 decreased by 13.4% compared with that of specimen CN-1. This is owing to the fact that the slab had less influence on the hogging moment, thus RBS directly reduced the hogging moment.

3.2.2 *Effect of RBS*

Although the concrete defects in specimen CS-1 were mainly responsible for the column failure, the increased bending moment capacity because of the slab might also be a reason. In contrast, due to the use of RBS, CS-5 showed a beam failure. The ductility coefficients for each specimen are presented in **Table 3**. The average ductility coefficient in two directions increased from 1.34 (CS-1) to 2.73 (CS-5) due to the effect of RBS. Developments of concrete cracks in the concrete slabs were also different for the two specimens. Only a few cracks were observed on the slab of specimen CS-1 due to the column failure mode, as shown in **Figure 14**. But the slab concrete in specimen CS-5 was crushed around the column and cracks were observed in almost a quarter of the beam span, as shown in **Figure 14**.

(a) CS-1 (b) CS-5

Figure 14. Concrete cracks and crushed concrete in slabs.

3.2.2 *Energy dissipation*

The capacity of energy dissipation is important in studying the seismic behaviour of joints. In general, the bigger the area of loop curves of the *P-Δ* relationship, the better the seismic behaviour of joints and the less potential fractures. The equivalent damping ratio (β) can reflect the energy dissipation

capacity of connections, as a function of $\beta = \frac{1}{2\pi}\frac{S_{ABCD}}{S_{OBE}+S_{ODF}}$, where S_{ABCDA}, S_{OBE}, S_{ODF} are the areas bounded by corresponding points, as shown in **Figure 15. Figure 16** shows the total accumulated energy (E_t) versus the accumulated relative displacement (Δ_a/Δ_y) relationships of three specimens. E_t is total energy absorbed by each specimen during the test, which is sum of the energy dissipation in each cycle. Δ_a is the accumulated displacement of beam tips.

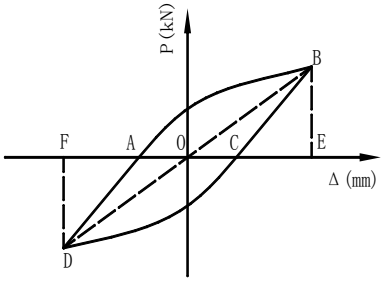

Figure 15. Calculation of equivalent damping ratio.

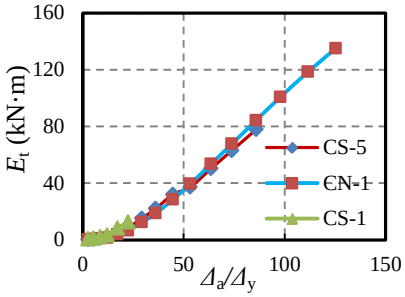

Figure 16. β versus Δ_a/Δ_y relationships.

Specimen No.	β	E_{total} (kN·m)
CN-1	0.46	135.02
CS-1	0.39	12.62
CS-5	0.42	97.79

Table 4. The joint's capacity of energy dissipation.

Specimen CS-1 failed very early; thus it could absorb very limited seismic energy of 12.62 kN·m. Compared with CS-1, the total dissipated energy by CS-5 increased to 97.79 kN·m. This confirms the beneficial influence of RBS on the energy dissipation capacity. Meanwhile, it is found the presence of the RC slab reduced the energy dissipation capacity of joints. The total accumulated energy of specimen CS-5 was only 57.6% of that of specimen CN-1. The equivalent damping ratio, as list in **Table 4**, also further confirms that the CFST column to steel beam joint (CN-1) has the best capacity of energy dissipation (β = 0.46), followed by the CFST column to RBS composite beam joint (β = 0.42), which increase by 8% compared with the joint composed of CSFT column and composite beam without the RBS (CS-1).

4 CONCLUSIONS

An experimental research was conducted to investigate whether the RBS can improve the seismic performance of composite joints and the influence of RC slab. It can be concluded that:

1) Two types of joint failure modes were observed, i.e., column failure (specimen CS-1) and beam failure (specimens CN-1 and CS-5). The presence of RC slab improves the strength of composite joints under sagging moment, but reduces the ductility and energy dissipation capacity of joints.

2) Using RBS in composite beam can improve both the ductility and energy dissipation capacity of joints due to the plastic hinge formation in the RBS region, which also prevents column failure.

3) The test results confirm that joints with RBS composite beams have a prospect to be applied in seismic regions. The joint with RBS composite beam had a ductility coefficient of 2.73 and an equivalent damping coefficient of 0.42, which shows that this type of joint have a good earthquake resistant capacity.

REFERENCES:

Cheng, C.T., Chan, C.F. & Chung, L.L. 2007. Seismic behavior of steel beams and CFT column moment-resisting joints with floor slabs. *Journal of Constructional Steel Research*. 63. 1479-1493.

Han, L.H. & Li, W. 2010. Seismic performance of CFST column to steel beam joint with RC slab: Experiments. *Journal of Constructional Steel Research*. 66, 1374-1386.

Liao, F.Y., Han, L.H. & Tao, Z. 2014. Behaviour of composite joints with concrete encased CFST columns under cyclic loading: Experiments. *Engineering Structures*. 59, 745-764.

SAC 1997. SAC protocol for fabrication, inspection, testing and documentation of beam-column joint. Sacramento (CA): SAC Joint Venture.